

Model of Nearshore Waves and Wave-Induced Currents around a Detached Breakwater

Pham Thanh Nam¹ and Magnus Larson²

Abstract: A numerical model that combines a random wave transformation and a wave-induced current model was developed in order to predict the wave and current fields around a detached breakwater. The wave field was determined using the EBED model, as reported by Mase in 2001, with a modified energy dissipation term. The surface roller associated with wave breaking was modeled based on a modification of the equations in works by Dally and Brown, and Larson and Kraus, in which the term for the roller energy flux in the alongshore direction was added to the energy balance equation. The nearshore currents and water elevation were determined from the continuity equation together with the depth-averaged momentum equations. The model was validated by three unique high-quality data sets obtained during experiments on detached breakwaters in the large-scale sediment transport facility basin at the Coastal and Hydraulics Laboratory in Vicksburg, Miss. The calculated significant wave height and longshore current were in good agreement with these measurements, whereas the cross-shore current was underestimated because undertow processes were not included in the modeling (depth-averaged equations employed). The calculated wave setup was somewhat overestimated; however, the absolute differences between the calculations and measurements were overall relatively small.

DOI: 10.1061/(ASCE)WW.1943-5460.0000038

CE Database subject headings: Breaking waves; Surf zones; Hydrodynamics; Nearshore; Water circulation; Breakwaters.

Author keywords: Breaking waves; Surf zone; Hydrodynamics; Nearshore circulation; Breakwaters.

Introduction

Detached breakwaters are frequently used to create favorable wave and current conditions in coastal areas. Thus, these structures are often employed for shore protection purposes since they reduce the longshore sediment transport generated by obliquely incident breaking waves preventing erosion along specific coastal stretches. A quantitative understanding of nearshore waves and currents in the vicinity of detached breakwaters is essential for the design and analysis of such structures with focus on the morphological evolution. Waves and currents mobilize, suspend, and transport sediment and gradients in the transport rate cause deposition or erosion of sediment, affecting the local bathymetry. A reliable and robust model of nearshore waves and currents is required to effectively predict sediment transport and the associated beach morphological evolution.

The wave energy balance equation is commonly applied for the prediction of multidirectional random wave transformation over large coastal areas. Originally, the nonstationary wave models WAM (WAMDI group 1988), and SWAN (Booij et al. 1996)

were based on the energy balance equation with source terms. However, diffraction was not included in these models, which made it difficult to apply them to coastal areas containing engineering structures. Mase (2001) introduced the diffraction term into the wave energy balance equation using a parabolic approximation. The wave transformation model thus derived, referred to here as the EBED model, is stable and can be applied to complex coastal areas containing structures. However, the experience of the writers, during this and previous modeling studies, is that predictions by the EBED model often overestimate wave heights in the surf zone. Thus, the EBED model was modified in the present study before applying it to calculate the nearshore wave conditions.

Much research has demonstrated that the surface roller plays an important role in the generation of nearshore currents and changes in the mean water level. The roller was first applied theoretically by Svendsen (1984a, b) to improve the modeling of wave setup and undertow in the surf zone. Dally and Brown (1995) further developed the roller model based on a depth-integrated and period-averaged energy balance equation. The model was validated with a number of laboratory data sets, which showed good agreement between computations and measurements. Larson and Kraus (2002) also applied this roller model in the NMLong numerical model, which was developed to simulate the longshore current across a single profile line. The wave energy dissipation per unit area after Dally et al. (1985) was substituted for the gradient of energy flux (per unit length of crest) in the x direction of the energy balance for the roller. In almost all previous studies, the energy balance for the rollers was only taken in the cross-shore direction. Recently, Tajima and Madsen (2006) enhanced the energy balance equation in two dimensions. However, despite this improvement, it is still difficult to estimate how much broken wave energy dissipation is transferred into the sur-

¹Doctoral Student, Dept. of Water Resources Engineering, Lund Univ., Box 118, SE-22100 Lund, Sweden; and, Researcher, Center for Marine Environment, Research and Consultation, Institute of Mechanics, Vietnamese Academy of Science and Technology, 264 Doi Can, Hanoi, Vietnam (corresponding author). E-mail: thanh_nam.pham@tvrl.lth.se

²Professor, Dept. of Water Resources Engineering, Lund Univ., Box 118, SE-22100 Lund, Sweden. E-mail: magnus.larson@tvrl.lth.se

Note. This manuscript was submitted on February 5, 2009; approved on September 30, 2009; published online on April 15, 2010. Discussion period open until October 1, 2010; separate discussions must be submitted for individual papers. This paper is part of the *Journal of Waterway, Port, Coastal, and Ocean Engineering*, Vol. 136, No. 3, May 1, 2010. ©ASCE, ISSN 0733-950X/2010/3-156-176/\$25.00.

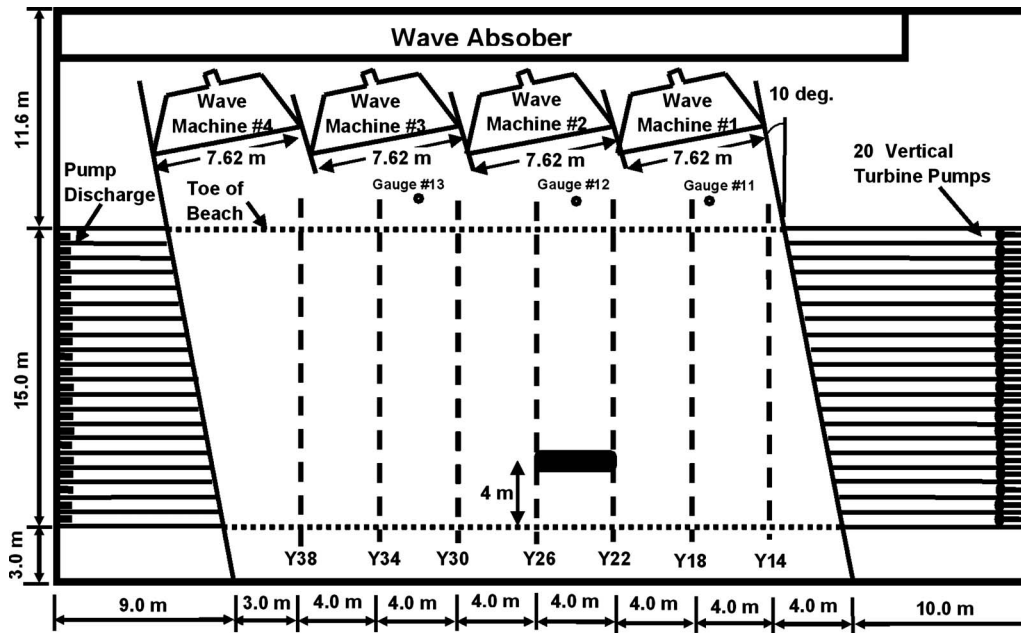


Fig. 1. Detached breakwater layout within LSTF for Tests 1 and 2 (Gravens and Wang 2007)

face roller, which decreases the accuracy in the calculation of the roller energy flux. In the present study, the approaches by Dally and Brown (1995) and Larson and Kraus (2002) were followed, and the energy flux term in the alongshore direction was included in the energy balance equation for the rollers.

There have been a number of studies on numerical models simulating the hydrodynamics in the vicinity of detached breakwaters. For example, Watanabe et al. (1986) simulated nearshore waves and currents around a detached breakwater and a groin, comparing the calculations with laboratory data. Péchon et al. (1997) employed seven numerical models for simulating the waves and currents in the vicinity of detached breakwaters, and intercompared them based on the laboratory data of Mory and Hamm (1997). However, these studies only dealt with regular waves and normal incidence. Sørensen et al. (1998) simulated the wave-induced horizontal nearshore circulation based on a time-domain Boussinesq-type model, and validated it with laboratory data. The computed wave height and wave setup were in good agreement with measurements for a limited number of profile lines. However, the comparison of calculated wave-induced currents with measurements was not detailed, especially for the test case on random waves. Zyserman and Johnson (2002) used a quasi three-dimensional model, dealing with random waves, to simulate flow, sediment transport, and morphological evolution.

Table 1. Offshore Wave Conditions

Data sets	Gauges	H_{mo} (m)	T_p (s)	θ (degrees)
T1C1	#11	0.219	1.442	6.5
	#12	0.236	1.470	6.5
	#13	0.226	1.459	6.5
T1C4	#11	0.222	1.452	6.5
	#12	0.232	1.472	6.5
	#13	0.225	1.464	6.5
T1C8	#11	0.219	1.457	6.5
	#12	0.236	1.468	6.5
	#13	0.224	1.461	6.5

Although the model produced reasonable-looking results of wave, current, and sediment transport, no validation was made due to lack of measurement data.

The objective of the present study was to develop a robust and reliable numerical model of nearshore waves and wave-induced currents, with the emphasis on coastal areas containing detached breakwaters. In order to do this, the wave energy dissipation due to wave breaking was modified in the energy balance equation of the EBED model. The modification resulted in better agreement between calculated and measured wave parameters for the data sets investigated. The two-dimensional creation and evolution of the surface roller associated with breaking waves was modeled based on an energy balance equation, which improved the prediction of radiation stresses due to rollers. These improvements then allowed for the development of a model of nearshore currents generated by random waves. In order to extend the model capability to a variety of conditions, including complex alongshore bathymetry, a general depth-averaged two-dimensional model of nearshore currents due to breaking waves, wind, and tides was developed. However, in the present paper the focus is on the wave-induced currents. The validation of the model developed was based on high-quality and synchronized data from experiments on detached breakwaters carried out in the large-scale sediment transport facility (LSTF) basin of the Coastal and Hydraulics Laboratory (CHL), U.S. Army Engineer Research and Development Center, in Vicksburg, Mississippi, United States.

Wave Model

Random Wave Model EBED

EBED is a multidirectional random wave transformation model, developed by Mase (2001) and based on the energy balance equation including energy dissipation and diffraction terms. The governing equation for steady state is expressed as follows:

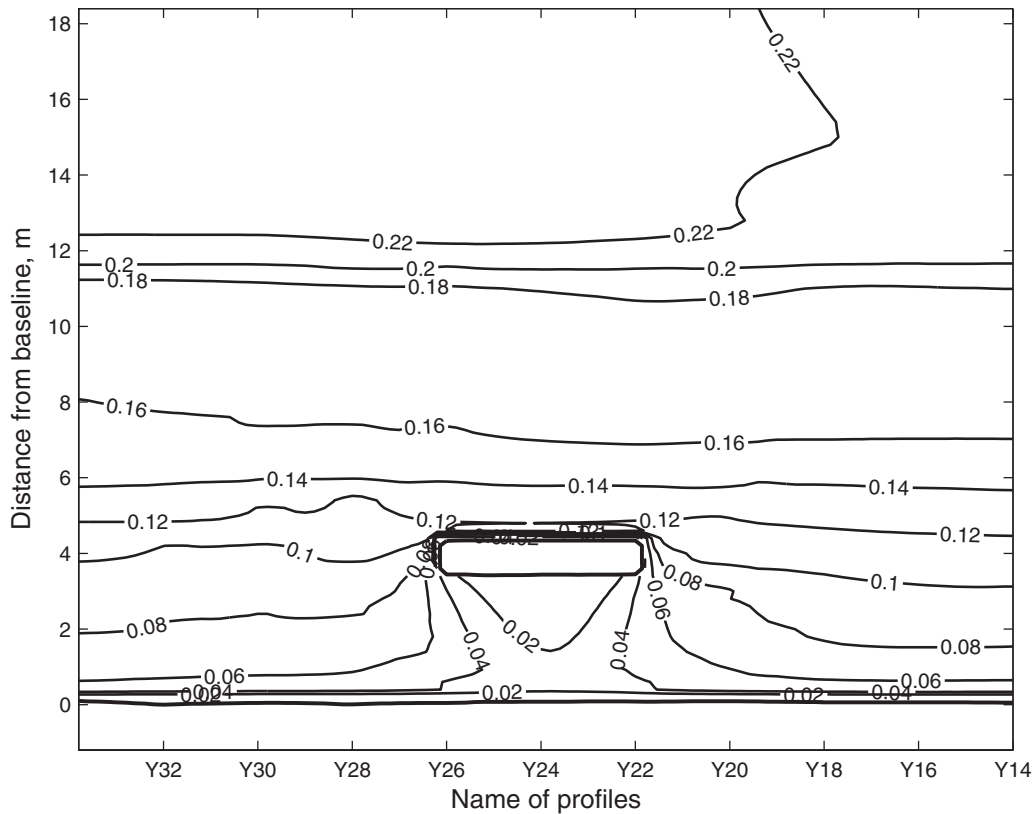


Fig. 2. Distribution of calculated significant wave height for LSTF Case T1C1

$$\frac{\partial(v_x S)}{\partial x} + \frac{\partial(v_y S)}{\partial y} + \frac{\partial(v_\theta S)}{\partial \theta} = \frac{\kappa}{2\omega} \left\{ (CC_g \cos^2 \theta S_y)_y - \frac{1}{2} CC_g \cos^2 \theta S_{yy} \right\} - \varepsilon_b S \quad (1)$$

where S =angular-frequency spectrum density; (x,y) =horizontal coordinates; θ =angle measured counterclockwise from the x axis; v_x , v_y , and v_θ =propagation velocities in their respective coordinate direction; ω =frequency; C =phase speed; and C_g =group speed. The first term on the right-hand side is added in the balance equation in order to represent the diffraction effects, and κ is a free parameter that can be optimized to change the influence of the diffraction effects. The second term represents the wave energy dissipation due to breaking waves, and ε_b is the energy dissipation coefficient. The output from the wave transformation model includes three main wave parameters: significant wave height H_s , significant wave period T_s , and mean wave direction $\bar{\theta}$ [for details see Mase (2001)].

Modified-EBED Model

The EBED model is stable and can be applied to complex beach topographies in coastal zones containing structures. However, it often overpredicts the wave heights in the surf zone compared to measurements. The overestimation is due mainly to the algorithm describing wave energy dissipation caused by wave breaking. In the EBED model, the energy dissipation coefficient is determined by the Takayama et al. (1991) model. The calculation of this coefficient is rather complex and the coefficient does not easily lend itself to calibration.

In this study, we modified the energy dissipation term based on the Dally et al. (1985) model in order to improve the predictive capability of the wave model in the surf zone. The modified energy balance equation proposed is as follows:

$$\frac{\partial(v_x S)}{\partial x} + \frac{\partial(v_y S)}{\partial y} + \frac{\partial(v_\theta S)}{\partial \theta} = \frac{\kappa}{2\omega} \left\{ (CC_g \cos^2 \theta S_y)_y - \frac{1}{2} CC_g \cos^2 \theta S_{yy} \right\} - \frac{K}{h} C_g (S - S_{stab}) \quad (2)$$

where h =still-water depth; K =dimensionless decay coefficient; and S_{stab} =stable wave spectrum density, which is a function of the stable wave height H_{stab} ($=\Gamma h$), with Γ being a dimensionless empirical coefficient. The model is referred to as the Modified-EBED model hereafter.

Several previous studies have dealt with the empirical coefficients Γ and K . The value of these coefficients can be given by constants, e.g., $\Gamma=0.4$ and $K=0.15$ (Dally et al. 1985), or empirical expressions containing the bottom slope [see Goda (2006) and Tajima and Madsen (2006)]. In the Modified-EBED model, a good description was obtained of the wave conditions in the surf zone for the LSTF data by modifying the expressions for the coefficients proposed by Goda (2006) as follows:

$$\begin{cases} \Gamma = 0.45, & K = \frac{3}{8}(0.3 - 19.2s): & s < 0 \\ \Gamma = 0.45 + 1.5s, & K = \frac{3}{8}(0.3 - 0.5s): & 0 \leq s \leq 0.6 \end{cases} \quad (3)$$

where s =bottom slope.

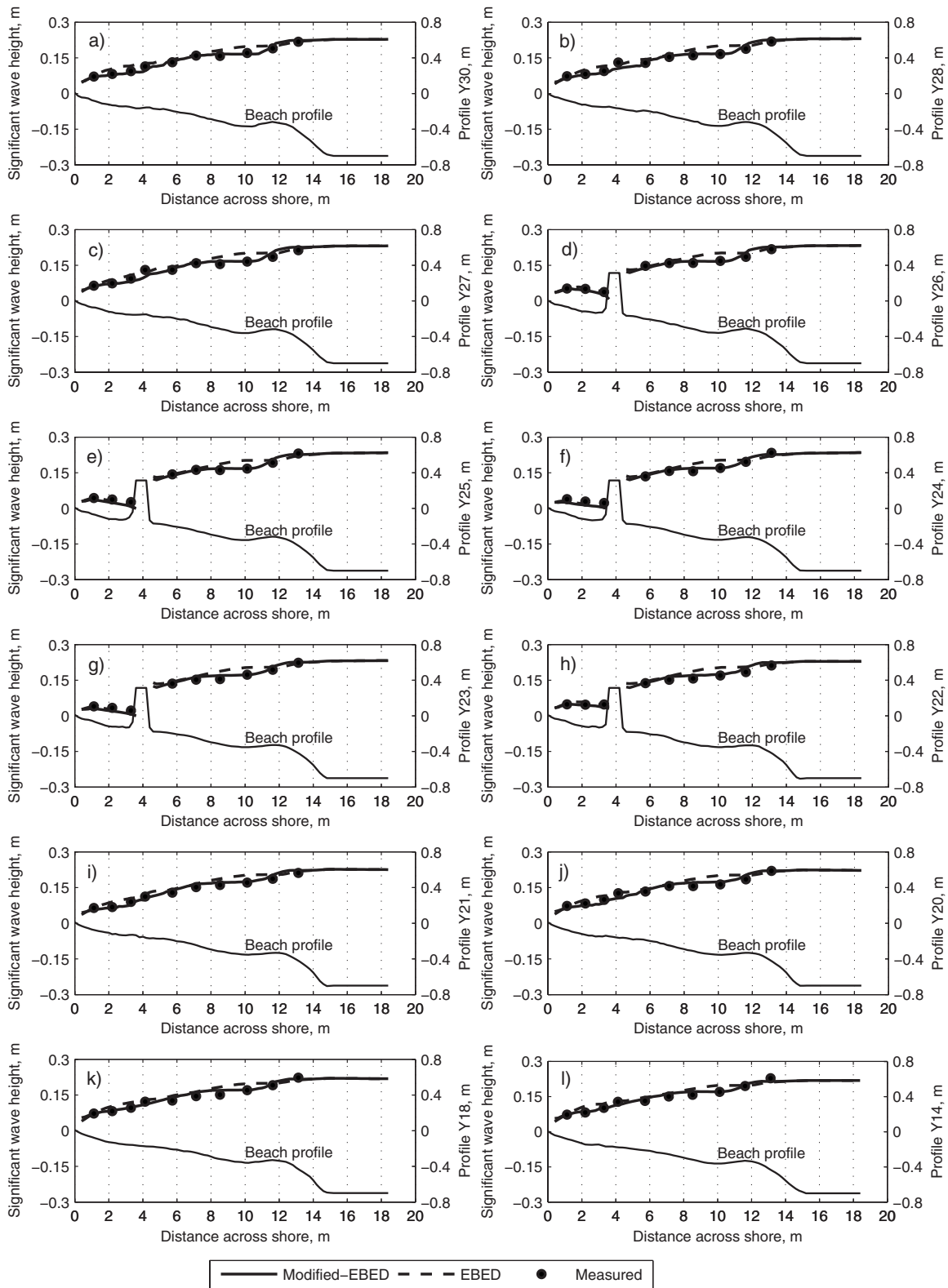


Fig. 3. Comparison of calculated and measured significant wave heights for LSTF Case TIC1

Surface Roller Model

The wave energy balance equation for surface rollers in two dimensions is expressed as (Dally and Brown 1995; Larson and Kraus 2002):

$$P_D + \frac{\partial}{\partial x} \left(\frac{1}{2} M C_r^2 \cos^2 \bar{\theta} \right) + \frac{\partial}{\partial y} \left(\frac{1}{2} M C_r^2 \sin^2 \bar{\theta} \right) = g \beta_D M \quad (4)$$

where P_D = wave energy dissipation $[=K C_g \rho g (H_{rms}^2 - (\Gamma h)^2) / (8h)]$; M = period-averaged mass flux; C_r = roller speed ($\approx C$); and β_D = roller dissipation coefficient.

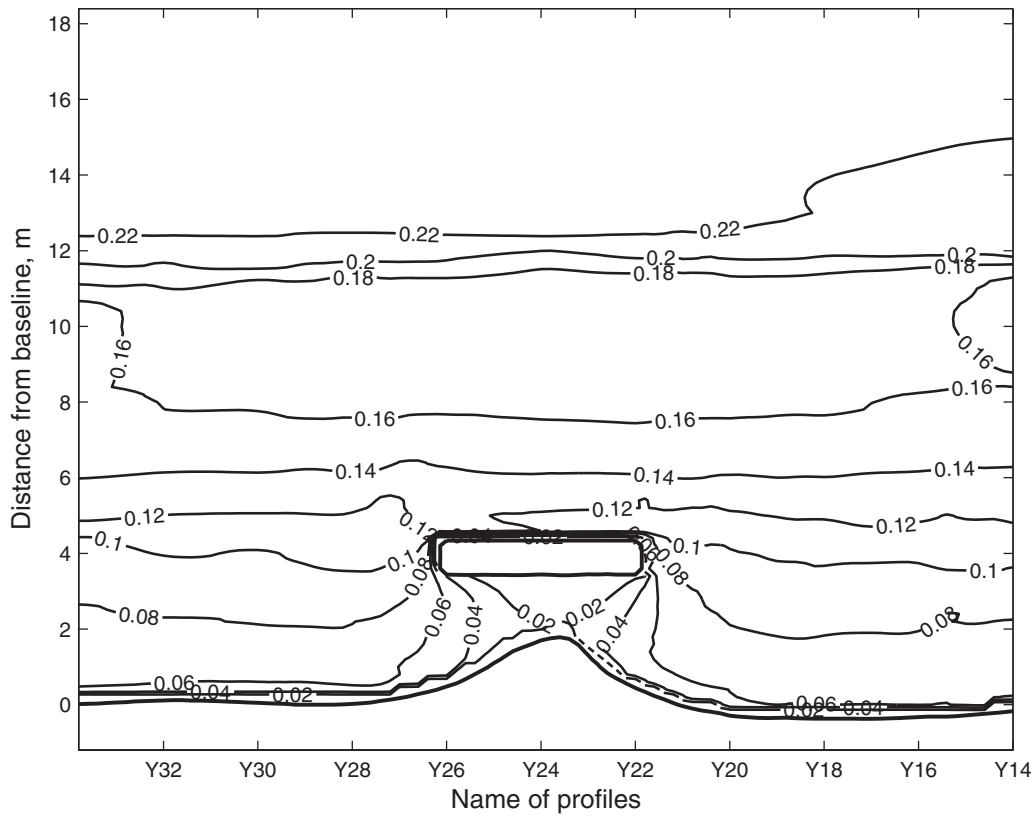


Fig. 4. Distribution of calculated significant wave height for LSTF Case TIC4

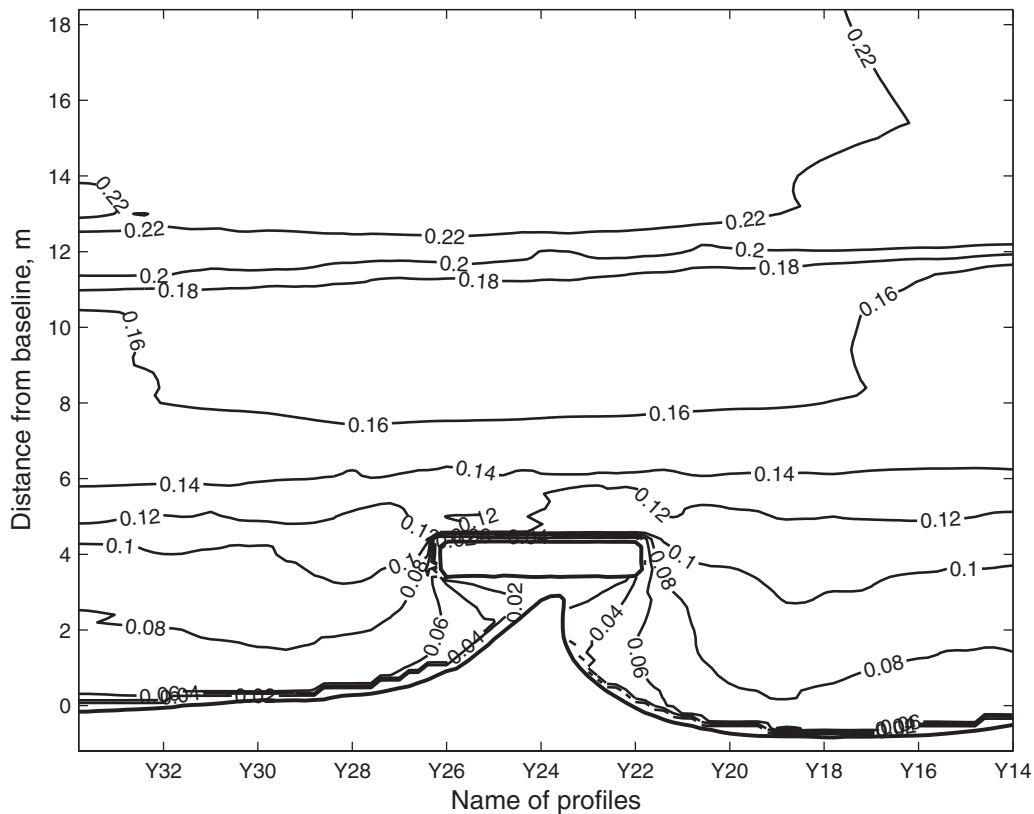


Fig. 5. Distribution of calculated significant wave height for LSTF Case TIC8

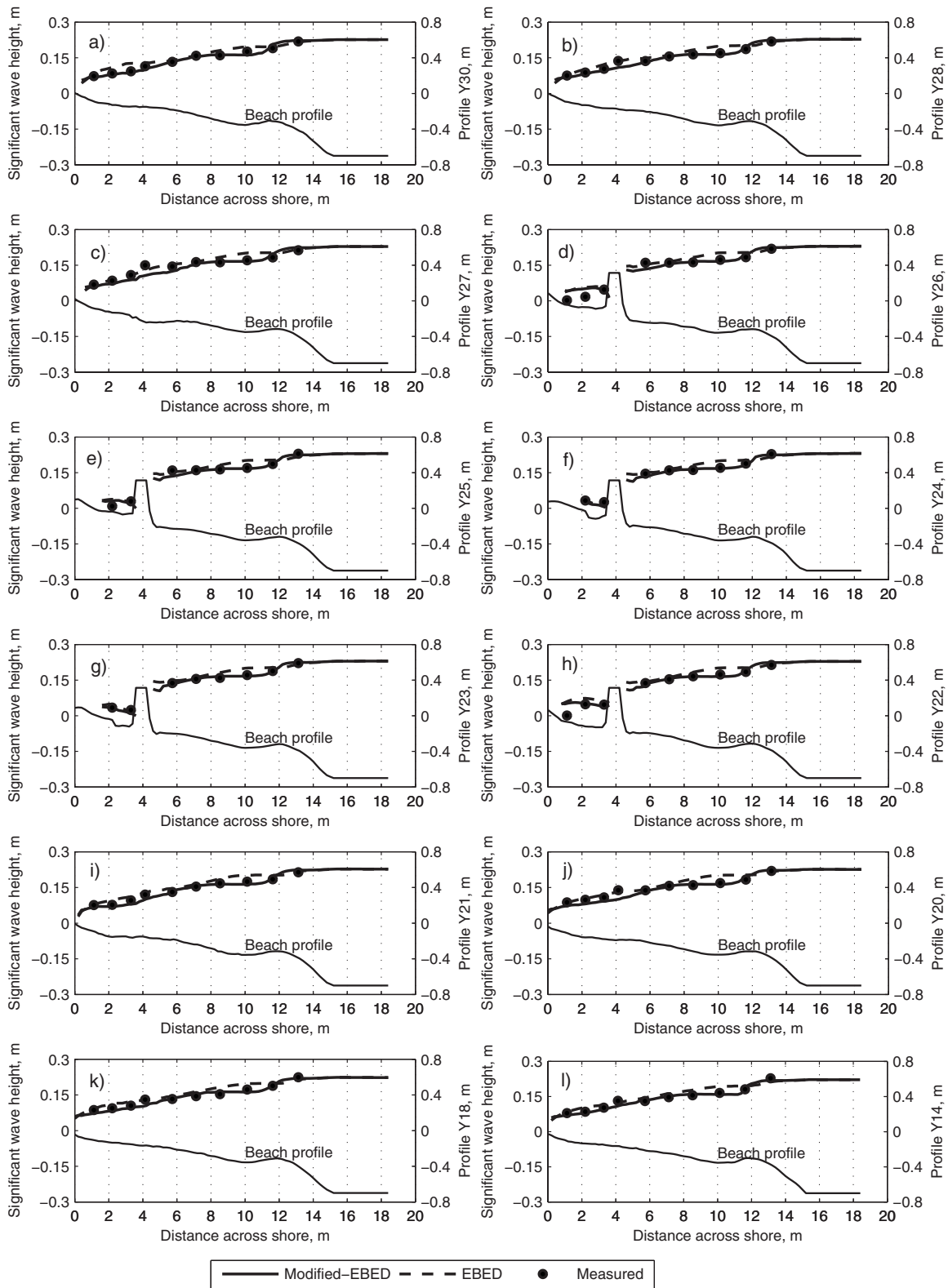


Fig. 6. Comparison of calculated and measured significant wave heights for LSTF Case TIC4

Nearshore Current Model

The governing equations for nearshore currents are written as (Militello et al. 2004)

$$\frac{\partial(h + \eta)}{\partial t} + \frac{\partial q_x}{\partial x} + \frac{\partial q_y}{\partial y} = 0 \quad (5)$$

$$\begin{aligned} \frac{\partial q_x}{\partial t} + \frac{\partial u q_x}{\partial x} + \frac{\partial v q_x}{\partial y} + g(h + \eta) \frac{\partial \eta}{\partial x} \\ = \frac{\partial}{\partial x} D_x \frac{\partial q_x}{\partial x} + \frac{\partial}{\partial y} D_y \frac{\partial q_x}{\partial y} + f q_y - \tau_{bx} + \tau_{Sx} \end{aligned} \quad (6)$$

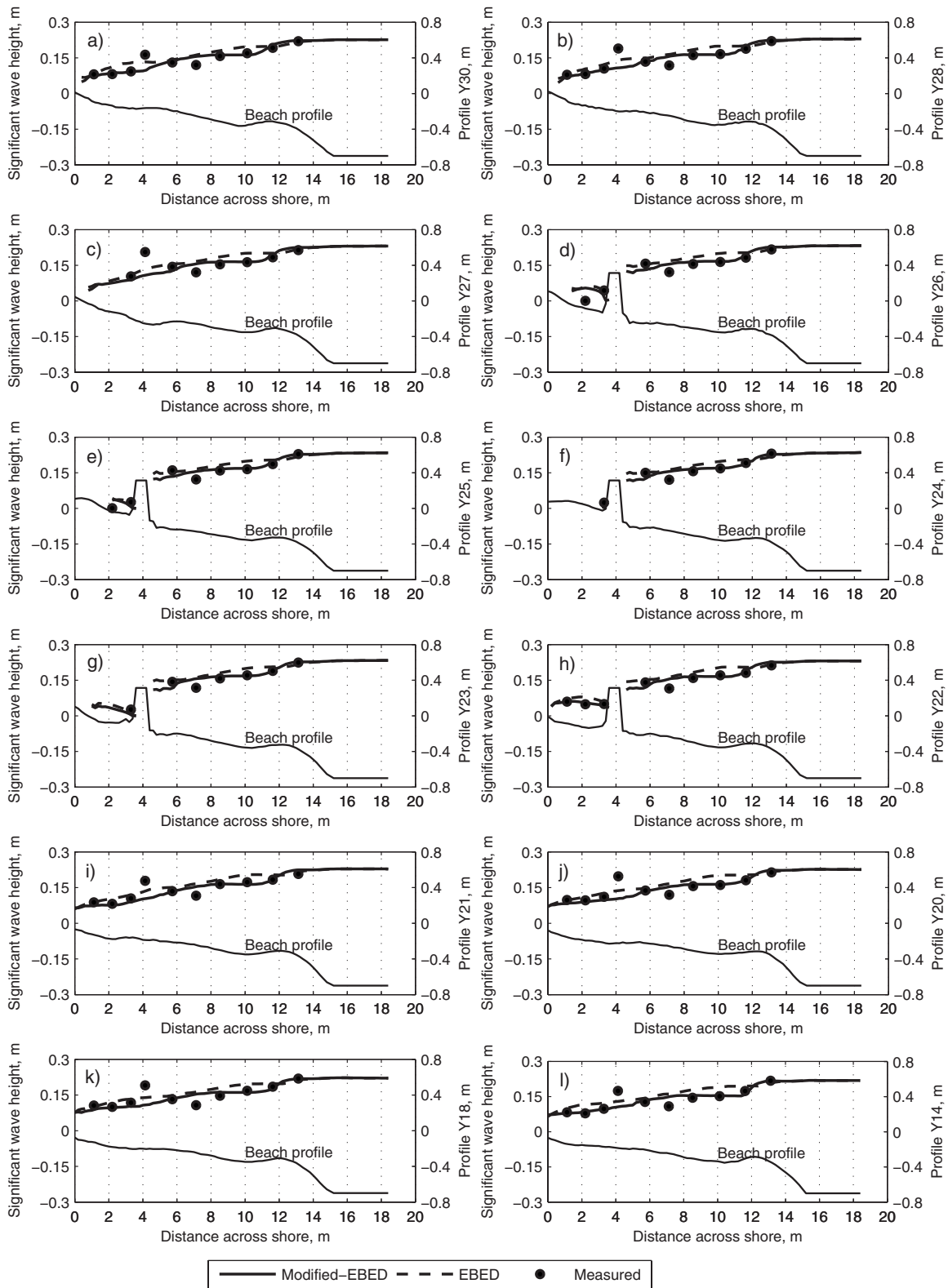


Fig. 7. Comparison of calculated and measured significant wave heights for LSTF Case TIC8

$$\begin{aligned} \frac{\partial q_y}{\partial t} + \frac{\partial u q_y}{\partial x} + \frac{\partial v q_y}{\partial y} + g(h + \eta) \frac{\partial \eta}{\partial y} \\ = \frac{\partial}{\partial x} D_x \frac{\partial q_y}{\partial x} + \frac{\partial}{\partial y} D_y \frac{\partial q_y}{\partial y} - f q_x - \tau_{by} + \tau_{Sy} \end{aligned} \quad (7)$$

where η =water elevation; q_x and q_y =flow per unit width parallel

to the x and y axes, respectively; u and v =depth-averaged velocity components in the x and y directions, respectively; g =acceleration due to gravity; D_x and D_y =eddy viscosity coefficients; f =Coriolis parameter; τ_{bx} and τ_{by} =bottom stresses; and τ_{Sx} and τ_{Sy} =wave stresses (the latter variables are all in the x - and y -directions, respectively).

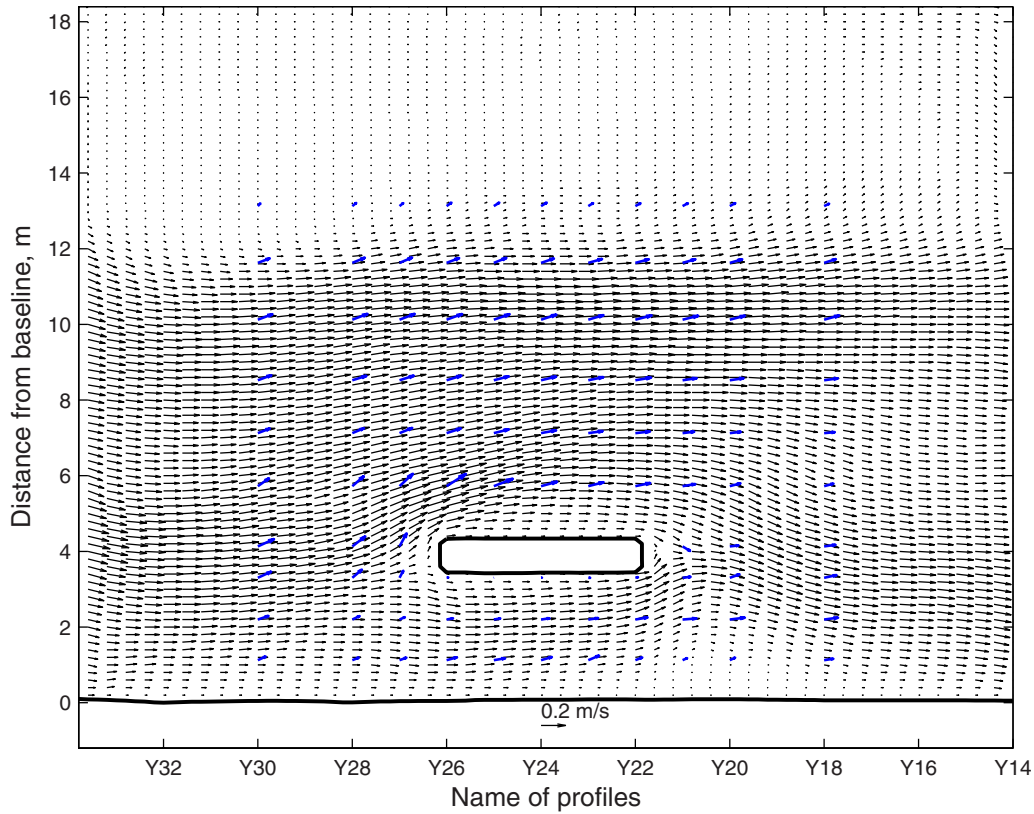


Fig. 8. Distribution of calculated and measured nearshore currents for LSTF Case T1C1

Outside the surf zone, the depth-averaged horizontal eddy viscosity coefficient can be calculated as a function of the total water depth, current speed, and bottom roughness according to Falconer (1980). In the surf zone, the eddy viscosity was taken to be a function of the wave properties following Kraus and Larson (1991). The bottom stresses under combined current and waves were determined from Nishimura (1988).

The wave stresses are derived from the wave transformation model and the surface roller model. They are given by the following equations:

$$\tau_{Sx} = -\frac{1}{\rho_w} \left[\frac{\partial}{\partial x} (S_{xx} + R_{xx}) + \frac{\partial}{\partial y} (S_{xy} + R_{xy}) \right] \quad (8)$$

$$\tau_{Sy} = -\frac{1}{\rho_w} \left[\frac{\partial}{\partial x} (S_{xy} + R_{xy}) + \frac{\partial}{\partial y} (S_{yy} + R_{yy}) \right] \quad (9)$$

where ρ_w = water density; S_{xx} , S_{xy} , and S_{yy} = wave-driven radiation stresses; and R_{xx} , R_{xy} , and R_{yy} = radiation stresses due to the roller. These stresses are determined from

$$S_{xx} = \frac{E}{2} [2n(1 + \cos^2 \bar{\theta}) - 1]; \quad S_{yy} = \frac{E}{2} [2n(1 + \sin^2 \bar{\theta}) - 1];$$

$$S_{xy} = S_{yx} = \frac{E}{2} n \sin 2\bar{\theta} \quad (10)$$

$$R_{xx} = MC_r \cos^2 \bar{\theta}; \quad R_{yy} = MC_r \sin^2 \bar{\theta}; \quad R_{xy} = R_{yx} = MC_r \sin 2\bar{\theta} \quad (11)$$

where $E = \rho_w g H_{rms}^2 / 8$ is the wave energy per unit area and $n = C_g / C =$ wave index.

LSTF Data

Five series of movable bed physical model experiments were conducted in the LSTF basin by Gravens et al. (2006) and Gravens and Wang (2007). A main objective of these experiments was to generate high-quality data sets for validating models to simulate the development of tombolos in the lee of nearshore detached breakwaters and T-head groins. The initial beach was constructed

Table 2. RMS Error (%) of Significant Wave Height, Longshore Current, Cross-Shore Current, and Wave Setup

Data sets	H_s modified-EBED	H_s EBED	v with roller	v without roller	u with roller	u without roller	η with roller	η without roller
T1C1	6.96	12.36	22.67	19.55	88.71	86.25	77.48	84.80
T1C4	8.39	11.75	35.73	34.24	92.66	82.97	83.65	94.13
T1C8	19.26	20.33	36.65	38.02	107.49	99.45	100.50	110.34

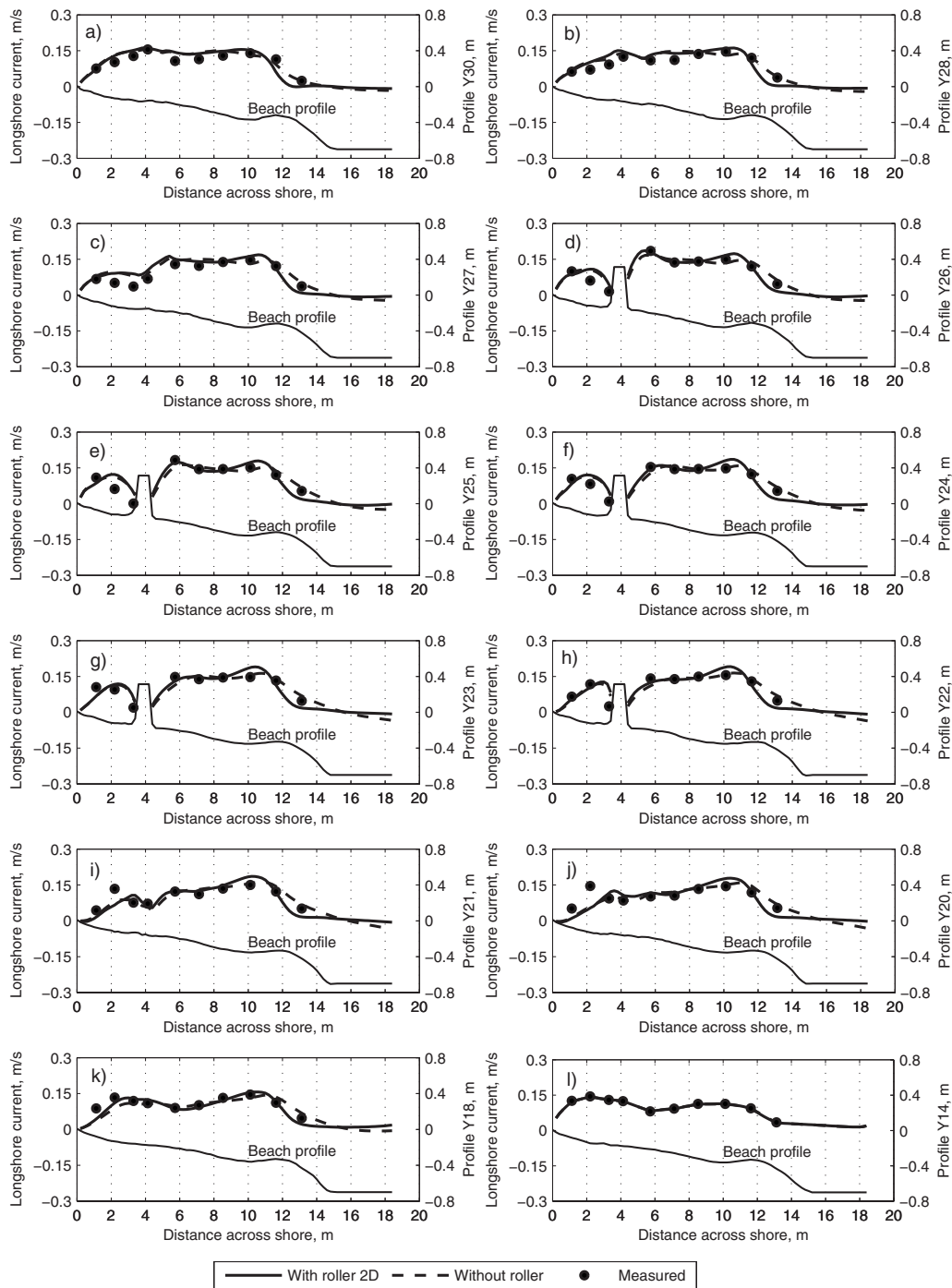


Fig. 9. Comparison of calculated and measured longshore currents for LSTF Case T1C1

with shore-parallel bottom contours and consisted of very well-sorted fine quartz sand with a median grain size of 0.15 mm. Four wave generators were programmed to produce spilling breaking waves in all experiments. The LSTF external pump system was used to maintain longshore current with a given cross-shore distribution.

Test 1 (T1), from which data were employed in this study, encompassed eight experimental runs of approximately 190 min each. In all these runs, a rubble-mound detached breakwater was used that was 4 m long and located 4 m from the initial still-water shoreline. The detached breakwater was constructed parallel to the initial shoreline (see Fig. 1). Three runs—T1C1, T1C4, and T1C8—were selected in order to evaluate the predictive capabil-

ity of the model regarding nearshore waves and currents corresponding to three morphological developments of the salient: (1) initial conditions with no salient; (2) distinct salient with the tip located approximately midway between the initial shoreline and the detached breakwater; and (3) salient close to equilibrium with its tip almost reaching to the detached breakwater (close to a tombolo).

The wave height, wave period, and wave setup were measured using 13 capacitance gauges, whereas the data on nearshore current were collected and measured by 10 acoustic-Doppler velocimeters (ADVs). Ten wave and current sensors were colocated in a cross-shore array on the instrumentation bridge. The ten locations were 1.125 m (ADV1), 2.725 m (ADV2), 3.3 (ADV3), 4.125 m

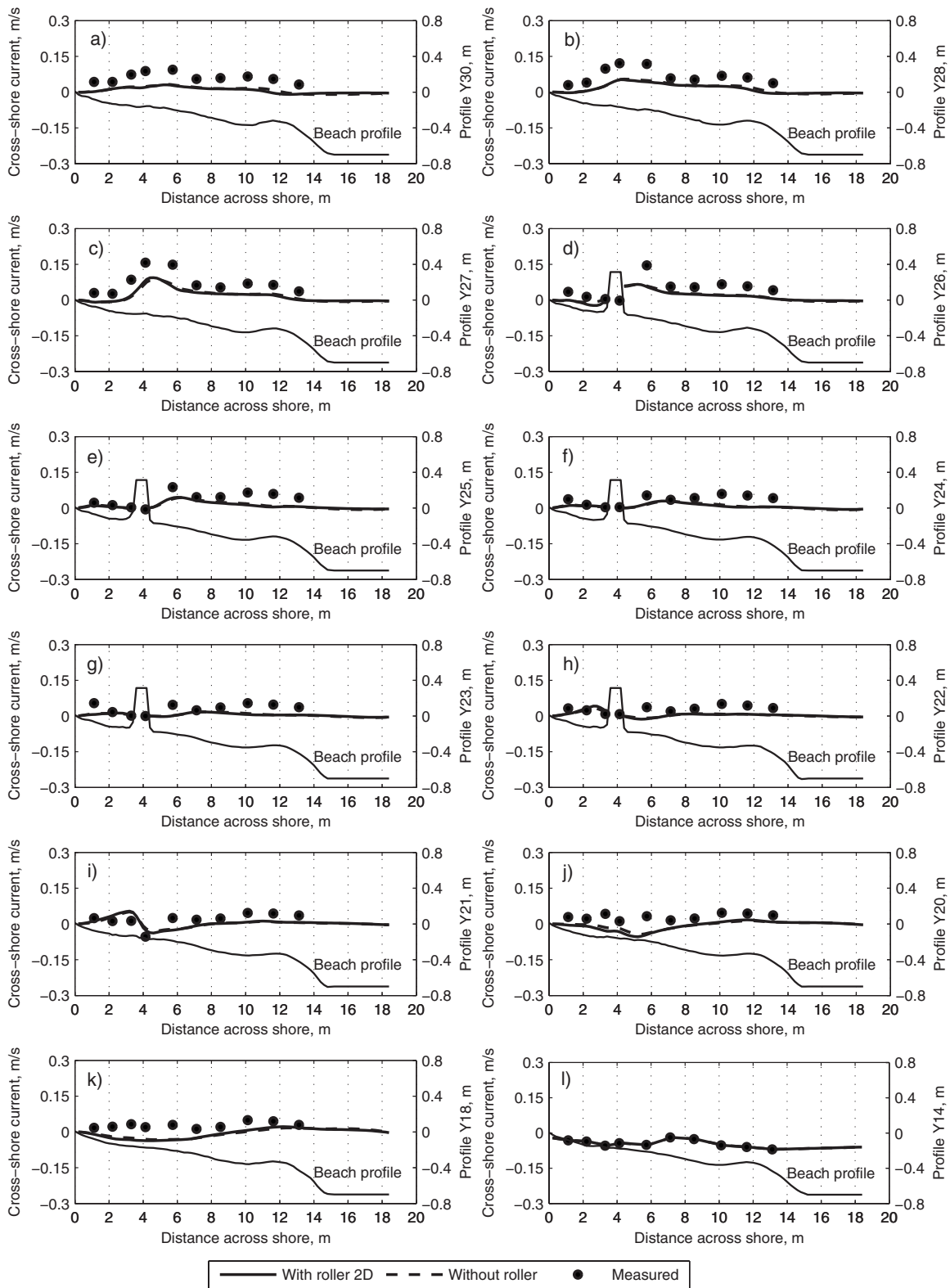


Fig. 10. Comparison of calculated and measured cross-shore currents for LSTF Case T1C1

(ADV4), 5.73 m (ADV5), 7.125 m (ADV6), 8.525 m (ADV7), 10.125 m (ADV8), 11.625 m (ADV9), and 13.125 m (ADV10) seaward from the initial still-water shoreline. To measure wave conditions seaward of the toe of the movable beach, the three

remaining wave sensors—Gauge#11, Gauge#12, and Gauge#13—were located at three alongshore positions, a distance 18.43 m seaward from the initial still-water shoreline (see Fig. 1).

The LSTF data employed to validate the model were collected

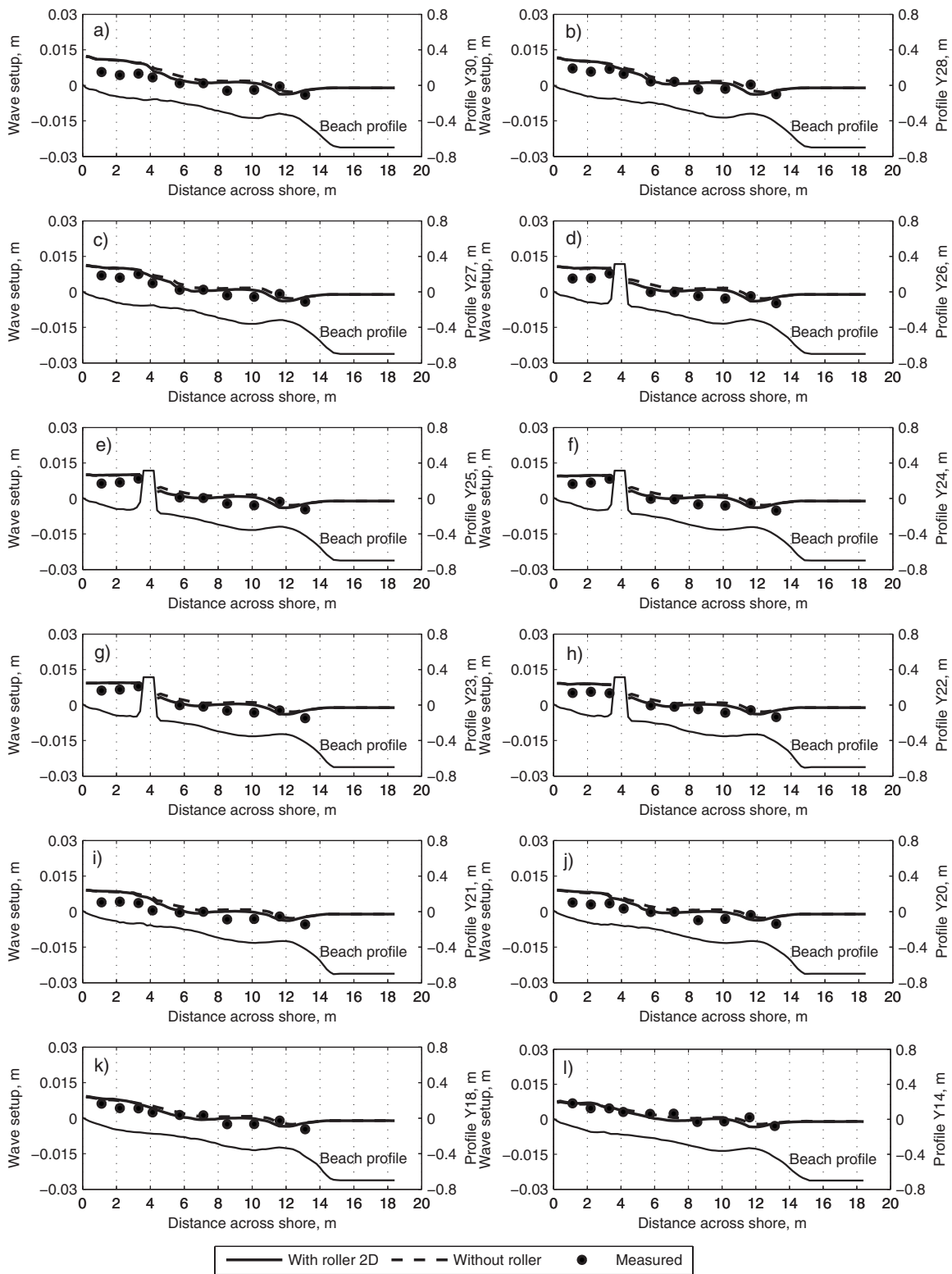


Fig. 11. Comparison of calculated and measured wave setups for LSTF Case T1C1

and analyzed by M. B. Gravens and P. Wang, personal communication, 2009. A Matlab routine using the semistandard power spectral density (PSD) and cross spectral density (CSD) (Welch 1967) functions were employed for spectral analyses of water level, current, and sediment concentration. Wave setup is the av-

erage water level over the 10-min sampling. The depth-averaged velocity is obtained by a simple averaging of the measured velocities at 3 to 8 levels through the water column. For more detailed information, see Wang et al. (2002a,b, 2003) and Wang (2006).

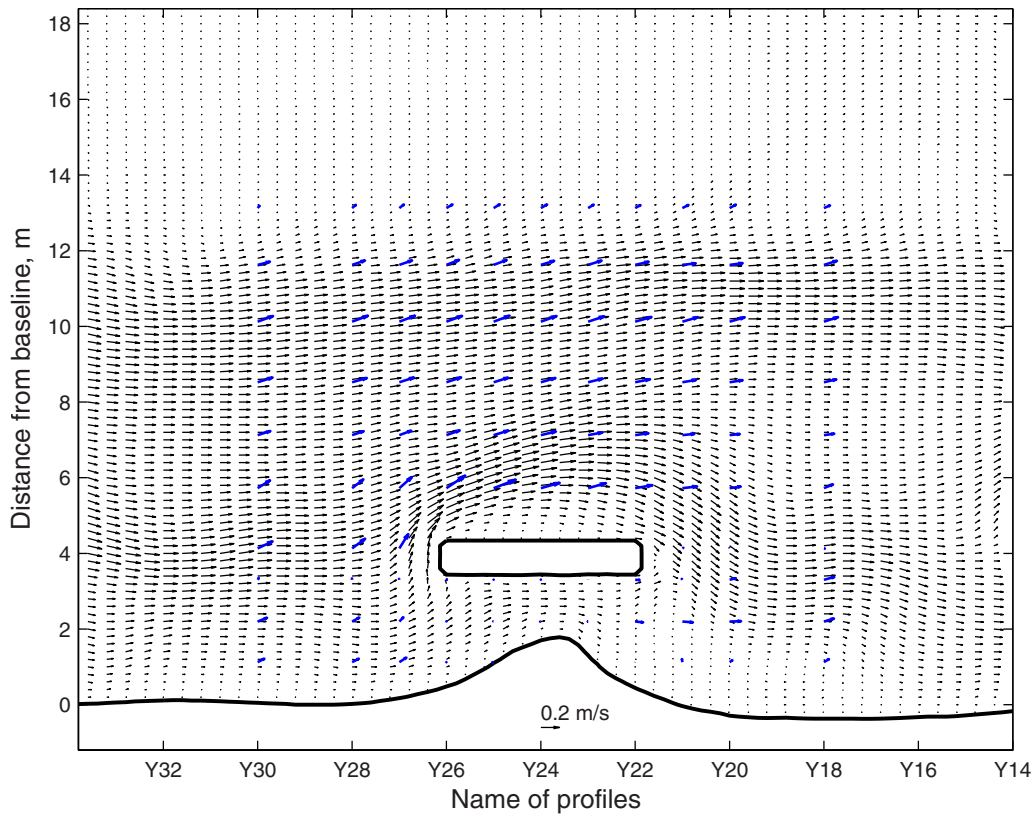


Fig. 12. Distribution of calculated and measured nearshore currents for LSTF Case TIC4

Comparison with LSTF Data

Comparison of Significant Wave Height

The computational grid for TIC1 was generated based on the beach profile data, from profile Y34 to profile Y14, through interpolation with a cell size 0.2×0.2 m. The wave measurements at Gauge#11, Gauge#12, and Gauge#13 were used as offshore wave conditions (model input). Detailed information of the offshore wave conditions at these points is presented in Table 1. A Texel, Marsen, and Arsløe (TMA) shallow-water spectrum was assumed at the offshore boundary with the parameter values $\gamma=3.3$, $\sigma_a=0.07$, $\sigma_b=0.09$, and the angular spreading of the waves $S_{\max}=25$. The decay and stable coefficients in the wave model were determined from Eq. (3).

Fig. 2 shows the spatial distribution of significant wave height obtained from the Modified-EBED model for TIC1. The wave diffraction effects are clearly seen behind the detached breakwater. Fig. 3 describes in detail the comparison between the computed results for the significant wave height and the corresponding measurements at 12 profile lines, from profile Y30 to profile Y14. The dashed line is the calculated significant wave height obtained with the original EBED model, which overestimated the wave height in the surf zone compared to the measured data, especially at ADV7 and ADV8 for all profile lines.

As can be seen, the Modified-EBED model based on a new approach for calculating wave energy dissipation produced improved results. The calculated significant wave height agreed well with the measured data at all measurement locations along the profile lines.

The computations of nearshore waves for TIC4 and TIC8 were carried out in the same manner as for TIC1. Figs. 4 and 5 show the contour lines of calculated significant wave height for TIC4 and TIC8, respectively. These figures clearly illustrate the impact of the salient development on the wave diffraction behind the detached breakwater. The simulations also demonstrated that the model remains stable in spite of the complex topography that develops behind the breakwater and that it produces robust and reliable results.

The detailed comparisons between the measured and calculated significant wave height along the 12 profile lines for TIC4 and TIC8 are presented in Figs. 6 and 7, respectively. As for TIC1, the wave predictions obtained with the Modified-EBED model were better than those by the original EBED model. As can be seen in the figures, the EBED model often overpredicts the wave heights at ADV7, ADV8, and ADV9. Although the significant wave height at some measurement locations near the shoreline was slightly underestimated by the Modified-EBED model, it successfully reproduced the significant wave height for both TIC4 and TIC8.

Quantitative assessment of the EBED and Modified-EBED models using the RMS error clearly shows that the modified model produced better agreement with the measured data. For example, the RMS error in the significant wave height obtained by the Modified-EBED model for TIC1 was only 6.96%, whereas it was 12.36% for the EBED model. For TIC8, the measurement of the significant wave height at ADV4 for several profile lines might not be correct [see Figs. 7(a–c and i–l)], thus it caused the RMS errors to become higher than that of TIC1 and TIC4. How-

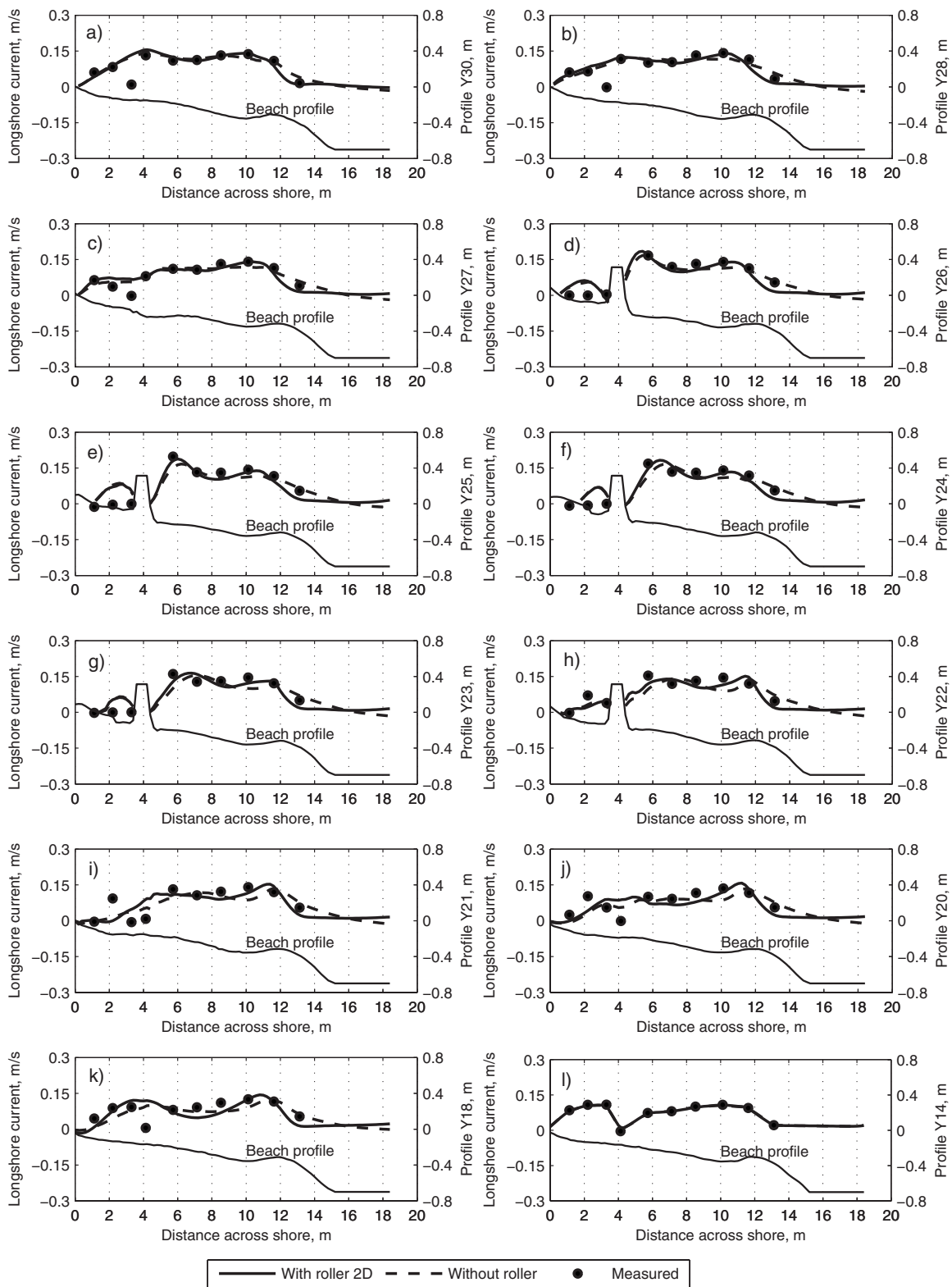


Fig. 13. Comparison of calculated and measured longshore currents for LSTF Case T1C4

ever, the RMS error for the significant wave height obtained using the Modified-EBED model (19.26%) was also better than that by the EBED model (20.33%). Table 2 summarizes in detail the RMS errors between computations and measurements for the significant wave height obtained by the EBED and the Modified-EBED model.

Mass Flux Obtained by 2D and 1D Surface Roller Model

The wave energy dissipation per unit area, P_D , was determined based on the RMS wave height, which can be derived from the wave calculations with the Modified-EBED model. The roller dis-

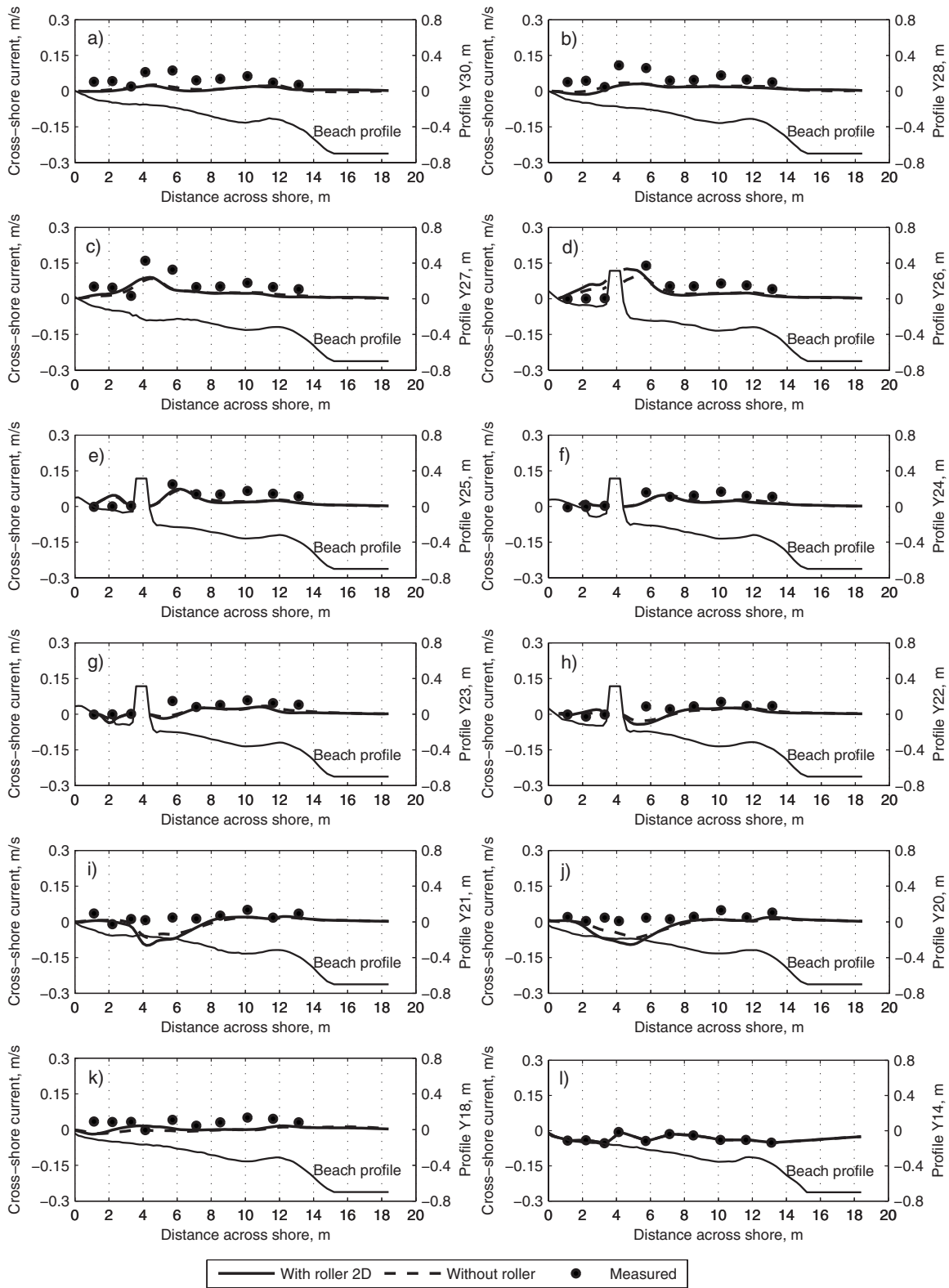


Fig. 14. Comparison of calculated and measured cross-shore currents for LSTF Case TIC4

sipation coefficient was set to 0.1 (Dally and Brown 1995). The maximum roller mass fluxes, M , obtained by Eq. (4) for TIC1, TIC4, and TIC8 were 9.33, 9.74, and 14.78 kg/m/s, respectively. If the energy flux term in the alongshore direction was neglected

in Eq. (4), giving rise to a 1D surface roller model, these maximum values of mass flux would change to 9.28, 8.35, and 13.58 kg/m/s, respectively.

The relative difference in roller mass flux obtained with the 2D

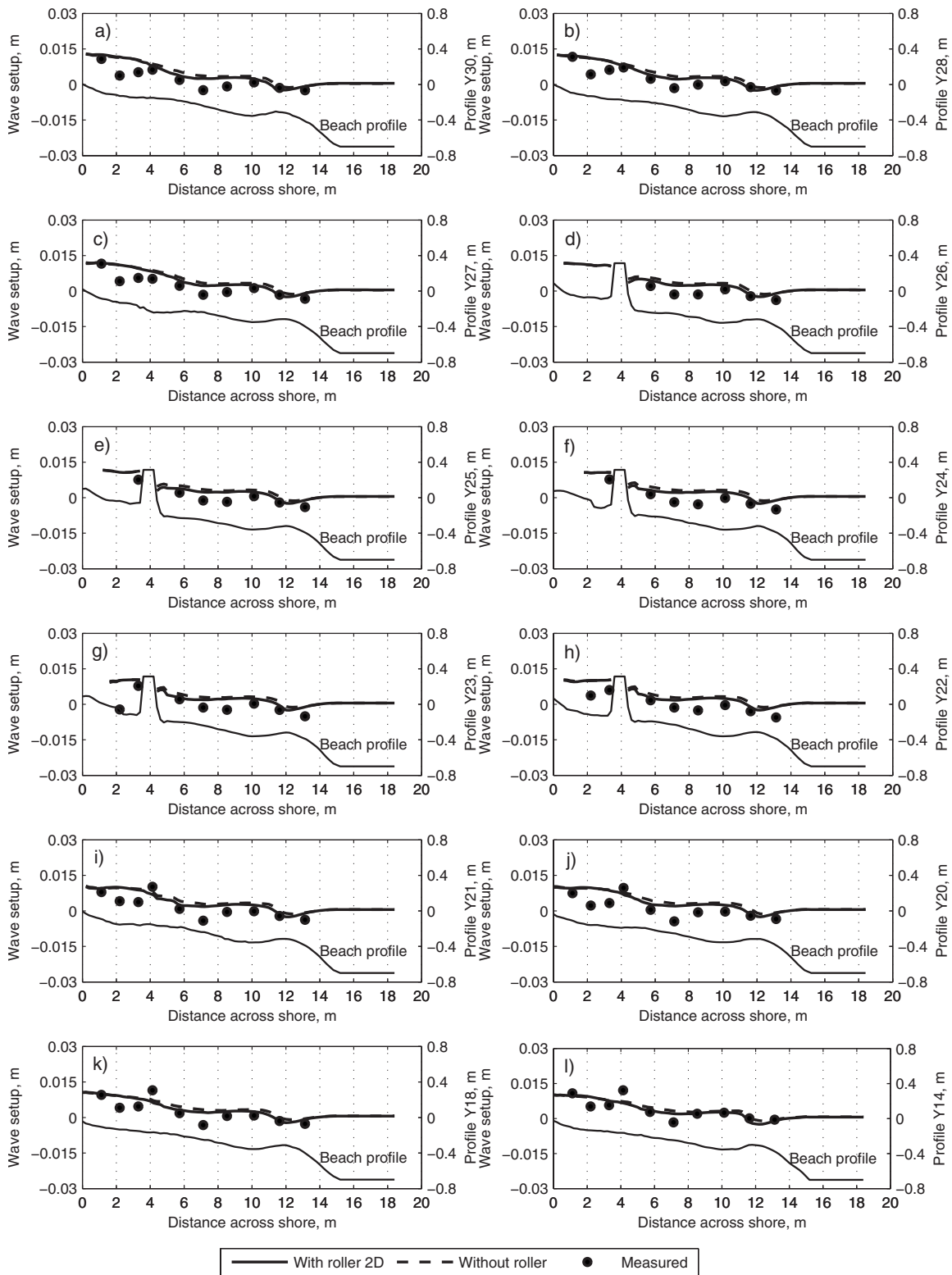


Fig. 15. Comparison of calculated and measured wave setups for LSTF Case T1C4

and 1D surface roller models for the test cases investigated was rather small. The maximum of the relative difference can be about 10% at some locations where the waves were broken. However, the absolute difference in mass flux was very small, implying that the difference between the wave stresses due to the roller obtained

by the 2D and 1D surface roller model for the investigated cases was not significant. Thus, for similar conditions it may be possible to employ a 1D instead of a 2D model to save time in the model execution, although this is something that has to be examined for the particular application.

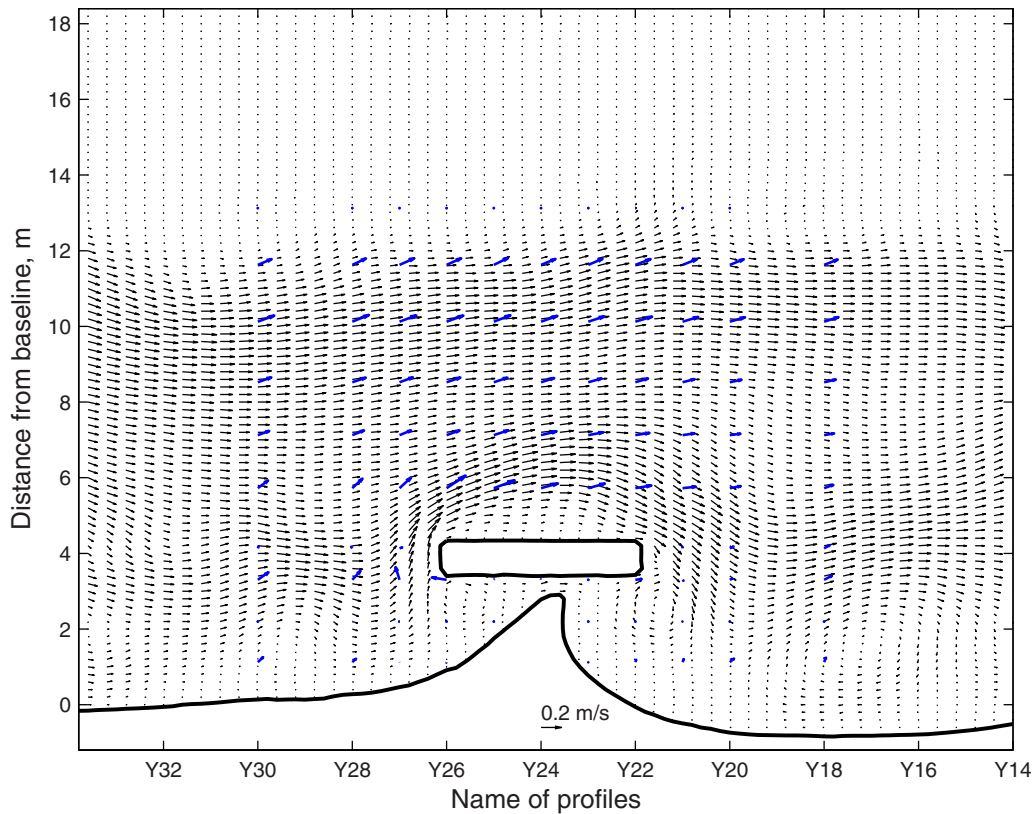


Fig. 16. Distribution of calculated and measured nearshore currents for LSTF Case TIC8

Comparison of Longshore Current, Cross-Shore Current, and Wave Setup

The output from the Modified-EBED model, including the significant wave height, wave direction, and wave period, was employed to calculate the nearshore current. The wave-driven stresses and the stresses due to the roller were derived from the Modified-EBED model and the surface roller model, respectively. The Manning coefficient was given as 0.025 to determine the bottom friction stresses. At both the upstream and downstream boundary, the water fluxes were given based on the measurement data of nearshore current on profiles Y34 and Y14. At the offshore boundary, the radiation boundary condition was employed (Reid and Bodine 1968).

Fig. 8 shows the spatial distribution of calculated and measured nearshore currents for TIC1. Note that the calculated vectors were plotted at 0.4-m interval in the alongshore direction, and measured vectors were presented by using the bold vectors. The calculation shows a small eddy was created on the right of the detached breakwater. Normally, two symmetric eddies are created in the lee of a detached breakwater, if the incident wave direction is perpendicular to the shoreline, the bathymetry is uniform in the alongshore direction, and the water fluxes are free to be transmitted through the lateral boundaries. However, in the TIC1 run, the incident waves were oblique to the shoreline, and the influx and outflux of water were specified at the upstream and downstream boundaries based on the measured velocities. Therefore, in the TIC1 run, only one eddy was created and it was shifted to the right in the lee of the detached breakwater.

Figs. 9 and 10 show the detailed comparison between the calculated and measured longshore current and cross-shore current with and without roller at the 12 profile lines for TIC1. Note that the longshore current is the velocity component parallel to the y

axis (with positive value when the flow is from left to right) and cross-shore current is the component perpendicular to this axis (with positive value in the offshore direction). The computational results show that the surface roller not only shifted the peak of the longshore current toward the shoreline but also increased the maximum current in the surf zone. As can be seen, the longshore current with and without roller agreed well with the measurements. The calculated cross-shore current with roller was quite similar to the one without roller, and the current agreed fairly well with measurements in the lee of the detached breakwater, although it underestimated the measurements at some profiles near the upstream and downstream boundaries. The main reason for the underestimation is probably that the undertow current was not accounted for in the model.

Fig. 11 compares the measured and computed wave setup for the 12 profile lines of TIC1. The calculated wave setup with roller was slightly different from that without roller. The model reproduced the wave setup well, although the setup tends to be overestimated compared to the measured data at ADV1, ADV2, and ADV3.

Fig. 12 illustrates the spatial distribution of the calculated and measured nearshore currents for TIC4. The calculated eddy to the right of the detached breakwater was larger and stronger than for TIC1 due to the salient. Fig. 13 shows the detailed comparison between the calculated and measured longshore current. As for TIC1, the model also produced good agreement with the measurement, especially for the locations seaward of the detached breakwater. However, the measured longshore current was small at ADV1, ADV2, and ADV3 from profile lines Y23 to Y26. The calculated longshore current overestimated measurements at these locations [see Figs. 13(d–g)].

The detailed comparison between the calculated and measured

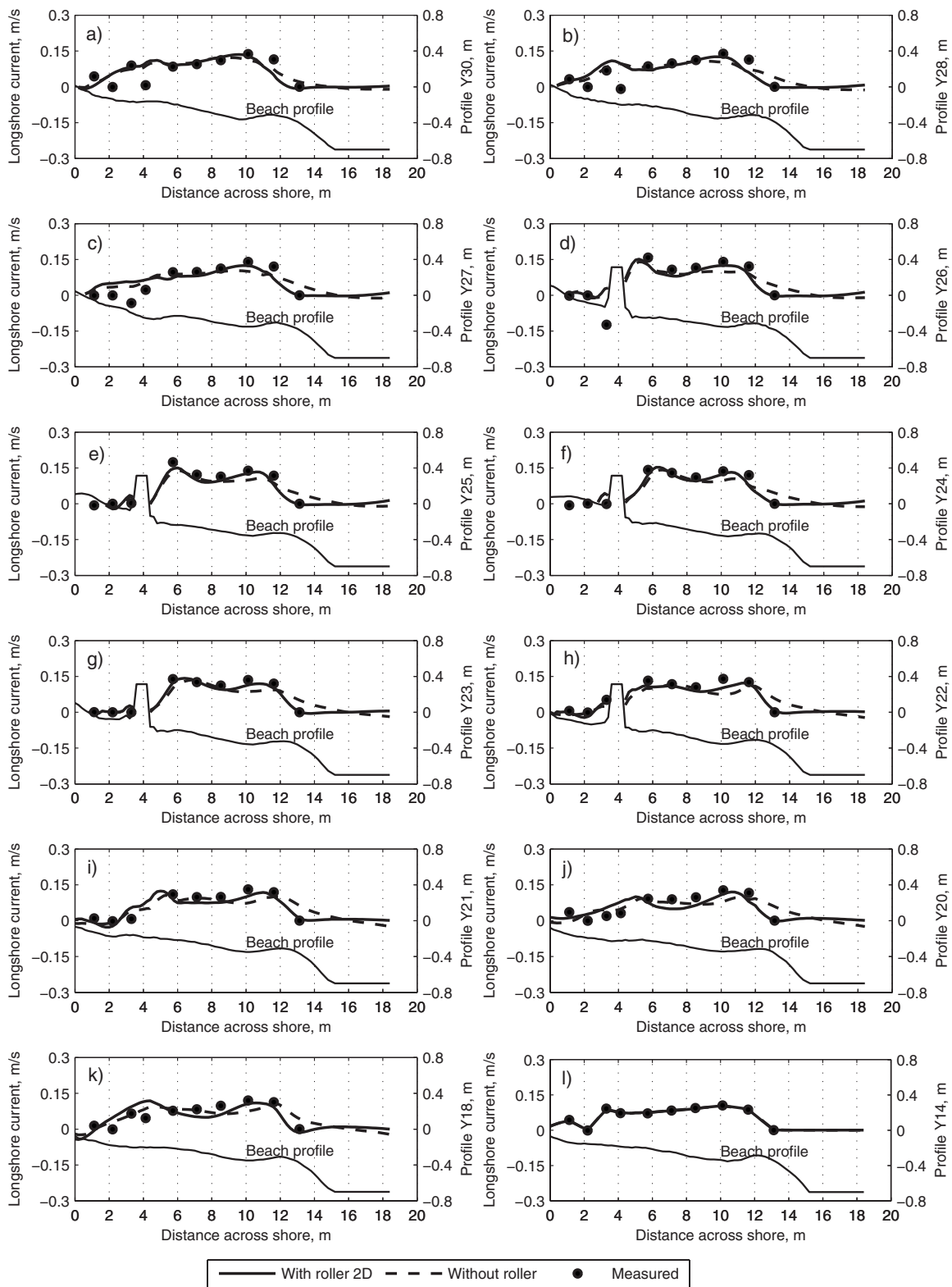


Fig. 17. Comparison of calculated and measured longshore currents for LSTF Case T1C8

cross-shore current for T1C4 is presented in Fig. 14. As for T1C1, the cross-shore current agreed fairly well with measurement in the lee of detached breakwater. The direction of the calculated cross-shore current was shoreward at ADV4, ADV5, and ADV6 of the profiles Y21 and Y20 [see Figs. 14(i and j)], where the measured current distribution was quite flat and close to zero. Again, the

likely explanation for this discrepancy is not including the undertow in the modeling, which would add a seaward contribution to the current under wave trough level.

Fig. 15 shows the comparison between calculated and measured wave setup for T1C4. In general, the calculated wave setup agreed fairly well with the measurements from ADV4 to ADV10,

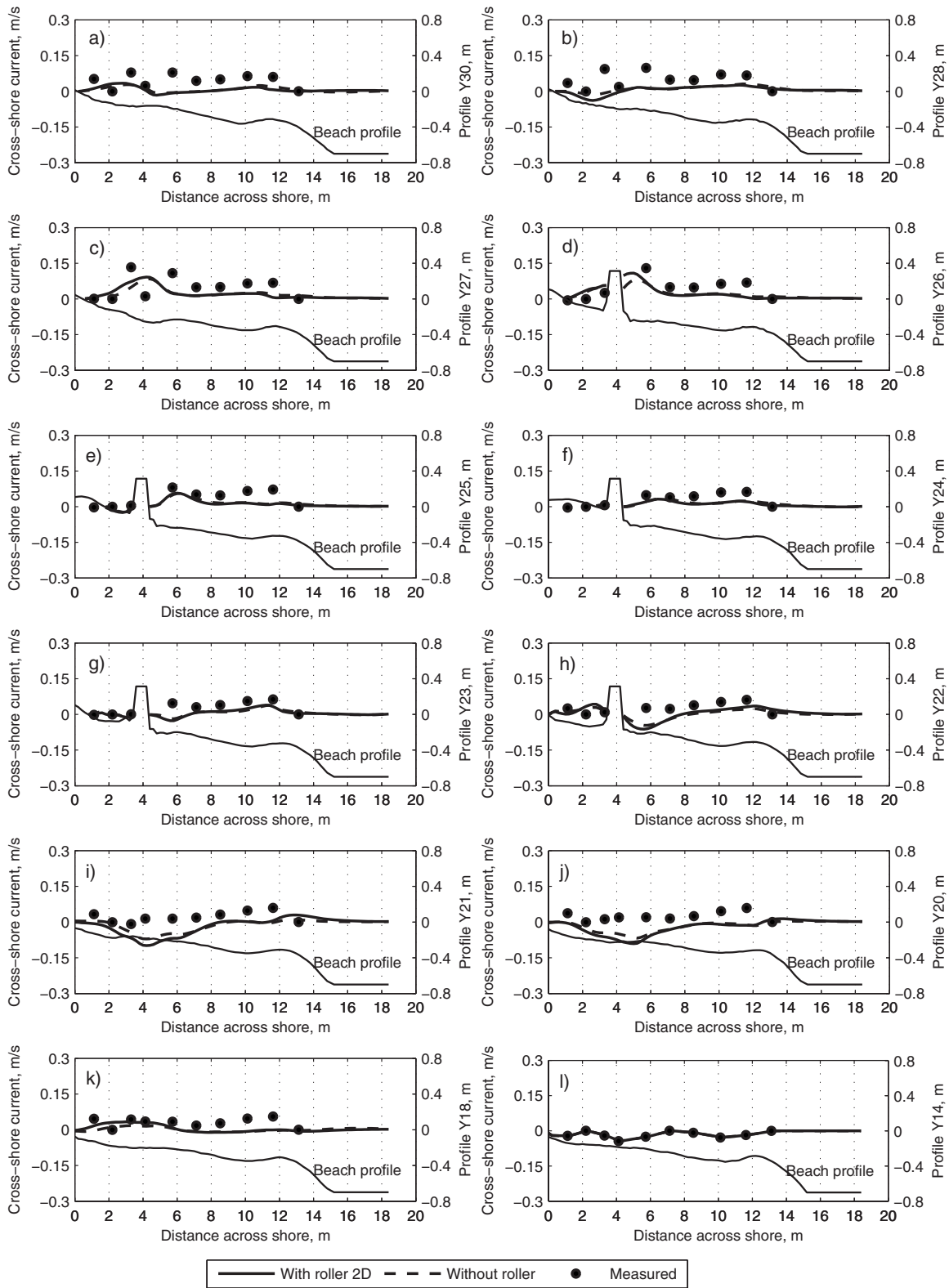


Fig. 18. Comparison of calculated and measured cross-shore currents for LSTF Case T1C8

but some overestimation occurred at ADV2 and ADV3. The wave setup was not observed at some locations in very shallow water behind the detached breakwater.

Fig. 16 shows the spatial distribution of the calculated and measured nearshore current for T1C8. Because the tip of the salient was close to the detached breakwater, the calculated

eddy was even stronger than for T1C4. Fig. 17 presents the detailed comparison between calculated and measured longshore current at the 12 profile lines. In general, the model reproduced rather well the longshore current observed in the measurement along all profile lines. The cross-shore computation was also in good agreement with measurement in the lee of detached break-

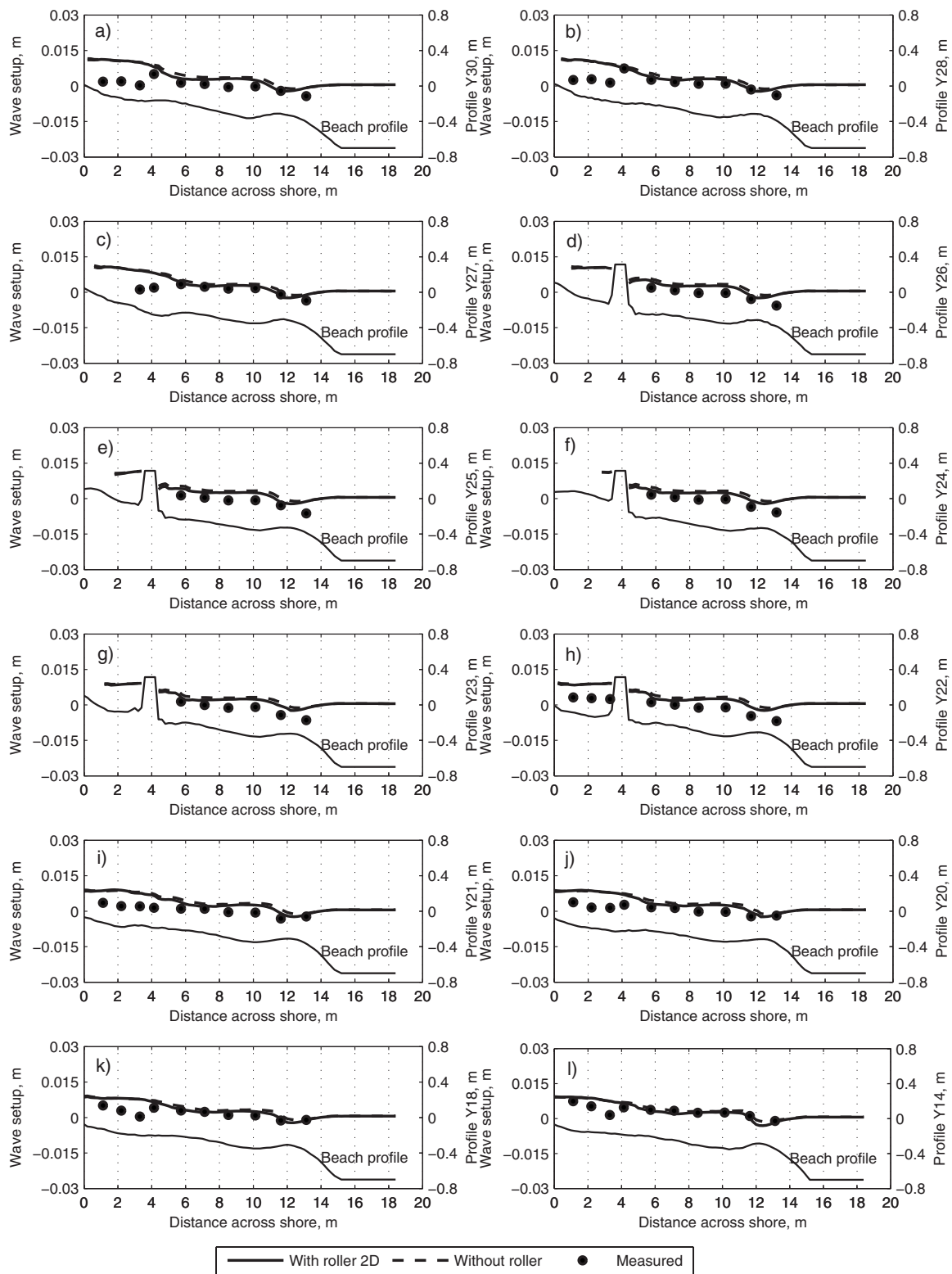


Fig. 19. Comparison of calculated and measured wave setups for LSTF Case T1C8

water [see Figs. 18(d-h)]. However, as for T1C4, the cross-shore current was underestimated compared to the measurements and had a shoreward direction at profiles Y21 and Y20 [Figs. 18(i and j)].

Fig. 19 illustrates the comparison between measured and calculated wave setup for T1C8. Similar to T1C4, the calculated wave setup was in quite good agreement with the measurements

from ADV4 to ADV10. In the very shallow water (ADV1, ADV2, and ADV3), the calculated wave setup overestimated the measurements. The gauges were probably recording in very shallow water, affecting the accuracy of the collected water levels.

A quantitative assessment of the agreement between measured and calculated longshore current, cross-shore current, and wave setup was also performed based on the RMS error between cal-

Table 3. Absolute Error (m) of Wave Setup

Data sets	η	η
	With roller	Without roller
T1C1	0.0019	0.0025
T1C4	0.0024	0.0031
T1C8	0.0032	0.0035

culations and measurements (see Table 2). For T1C1 and T1C4, the RMS errors of longshore current without roller were slightly better than those with roller. The calculated cross-shore current agreed fairly well with the measurements in the lee of the detached breakwater, but underestimated the current at the remaining measurement locations, causing larger RMS errors.

In addition, the absolute error was also used to compare the wave setup calculations with the measurements. Table 3 summarizes in detail the absolute error in the wave setup for the three investigated test cases. Although the relative RMS error of wave setup was quite large, the absolute error was relatively small. For example, in test case T1C1, the RMS errors of wave setup with and without roller were 77.48% and 84.80%, respectively. However, the corresponding absolute errors were only 0.0019 and 0.0025 m.

Discussion

This study involved a modification of the energy dissipation calculation due to breaking used in the EBED model developed by Mase (2001). The modification was based on Dally et al. (1985), producing a significant improvement in calculating the wave conditions in the surf zone. As a result, the Modified-EBED is able to provide more accurate input for the numerical model used to simulate the nearshore currents, as well as for models employed to determine the sediment transport and morphological evolution.

The importance of the roller in calculating wave-induced currents was also investigated. Roller effects not only shifts the peak of the longshore current toward the shoreline, but they also increase the magnitude of the longshore current in the surf zone. By using a 2D surface roller model, energy conservation was expressed more accurately than with the 1D model. For the three test cases from the LSTF data investigated, the difference in roller mass fluxes obtained by 2D and 1D surface model was small. However, the 2D surface roller model should be employed for areas with complex bathymetry and high wave energy in order to obtain more accurate wave-induced currents.

The absolute error in wave setup was small, although a large relative error was obtained. For the LSTF data, the instrument errors were quite small, typically less than 2% (M. B. Gravens and P. Wang, personal communication, April 28, 2009), and all the instruments were checked before the measurements. However, the measurements at some locations near the shoreline were difficult to carry out due to very shallow water and the wave and current sensors could be over the water surface. Furthermore, the air bubbles from breaking waves penetrated into the water column potentially affecting the observed values (Hamilton and Ebersole 2001). Therefore, the RMS errors in the wave setup were quite large at certain measurement locations for the three investigated test cases.

The numerical models for nearshore waves and wave-induced currents employed several empirical coefficients that could be specified with confidence and that have potential for general ap-

plicability. The decay and stable coefficients, which were determined by Eq. (3), produced good results regarding the wave field for the LSTF data. However, these equations should be validated with other laboratory and field data to ensure their general applicability. The roller dissipation and the bottom friction coefficients directly affect the speed and the cross-shore distribution of longshore currents. In the present study, the value of the roller dissipation coefficient was set to 0.1 following the recommendation of Dally and Brown (1995), and the Manning coefficient was given as 0.025 to determine the bottom friction based on calibration. These values provided good agreement between the computations and the measurements. The eddy viscosity coefficients, which were determined by Falconer (1980) and Kraus and Larson (1991), make the cross-shore variation in wave-induced current smoother, but their effects on the current magnitude is relatively small.

Conclusions

The present study represents one of the first attempts to validate, in a comprehensive manner, a numerical model developed for predicting the wave and current field around a detached breakwater. Such a model is a necessary component in any system to simulate the bathymetric evolution in response to nearshore structures in the coastal zone.

A general, robust, and reliable numerical model was developed to predict nearshore waves and currents in coastal areas with structures present that induce complex topographic conditions. The energy dissipation algorithm for wave breaking in the multidirectional random wave transformation model EBED (Mase 2001) was modified after Dally et al. (1985), producing more accurate wave fields in the surf zone. The creation and evolution of surface roller was employed and enhanced based on the model of Dally and Brown (1995) and Larson and Kraus (2002) in order to improve the wave radiation stresses in the surf zone. The nearshore currents and water elevation were determined from the continuity equation together with the depth-averaged momentum equations.

The developed model was validated by employing high-quality data sets from three experimental test cases in the LSTF basin involving a detached breakwater (Gravens et al. 2006; Gravens and Wang 2007). These simulations showed that the model well reproduced the significant wave height and longshore current at all measured locations. The calculated cross-shore current underestimated the measurements along several profile lines, probably because the undertow was not included in the model. Although the calculated wave setup often overestimated the measurements, the absolute error was relatively small. Therefore, the model is expected to provide reliable input for calculating the sediment transport and morphological evolution in the vicinity of coastal structures due to waves and currents.

Acknowledgments

This work was partly funded by Sida/SAREC in the framework of the Project VS/RDE/03 "The evolution and sustainable management in the coastal areas of Vietnam," partly by Lars Erik Lundbergs Scholarship Foundation, and partly by the Inlet Modeling System Work Unit of the Coastal Inlets Research Program, U.S. Army Corps of Engineers. Dr. Hajime Mase at Kyoto University kindly supplied the source code for the EBED model. Dr. Ping

Wang at University of South Florida and Mr. Mark Gravens at CHL provided the experimental data from their tests, which is greatly appreciated. The writers thank Mrs. Margaret Newman-Nowicka at Lund University for her useful language comments. The writers thank Dr. Nguyen Manh Hung, and the late Prof. Pham Van Ninh for their great contributions to the Project VS/RDE/03 and comments on early drafts of this paper. Finally, the writers thank the anonymous reviewers for their valuable comments.

References

- Booij, N., Holthuijsen, L. H., and Ris, R. C. (1996). "The 'SWAN' wave model for shallow water." *Proc., 25th Int. Conf. on Coastal Engineering*, ASCE, New York, 668–676.
- Dally, W. R., and Brown, C. A. (1995). "A modeling investigation of the breaking wave roller with application to cross-shore currents." *J. Geophys. Res.*, 100(C12), 24873–24883.
- Dally, W. R., Dean, R. G., and Dalrymple, R. A. (1985). "Wave height variation across beaches of arbitrary profile." *J. Geophys. Res.*, 90(C6), 11917–11927.
- Falconer, R. A. (1980). "Modelling of planform influence on circulation in harbors." *Proc., 17th Int. Conf. on Coastal Engineering*, ASCE, New York, 2726–2744.
- Goda, Y. (2006). "Examination of the influence of several factors on longshore current computation with random waves." *Coastal Eng.*, 53, 157–170.
- Gravens, M. B., and Wang, P. (2007). "Data report: Laboratory testing of longshore sand transport by waves and currents; morphology change behind headland structures." *Technical Rep. No. ERDC/CHL TR-07-8*, Coastal and Hydraulics Laboratory, U.S. Army Engineer Research and Development Center, Vicksburg, Miss.
- Gravens, M. B., Wang, P., Kraus, N. C., and Hanson, H. (2006). "Physical model investigation of morphology development at headland structures." *Proc., 30th Int. Conf. on Coastal Engineering*, World Scientific, Singapore, 3617–3629.
- Hamilton, D. G., and Ebersole, B. A. (2001). "Establishing uniform longshore currents in large-scale sediment transport facility." *Coastal Eng.*, 42(3), 199–218.
- Kraus, N. C., and Larson, M. (1991). "NMLONG: Numerical model for simulating the longshore current; report 1: Model development and tests." *Technical Rep. No. DRP-91-1*, U.S. Army Engineer Waterways Experiment Station, Vicksburg, Miss.
- Larson, M., and Kraus, N. C. (2002). "NMLONG: Numerical model for simulating longshore current; report 2: Wave-current interaction, roller modeling, and validation of model enhancements." *Technical Rep. No. ERDC/CHL TR-02-22*, U.S. Army Engineer Research and Development Center, Vicksburg, Miss.
- Mase, H. (2001). "Multi-directional random wave transformation model based on energy balance equation." *Coast. Eng. Japan*, 43(4), 317–337.
- Militello, A., Reed, C. W., Zundel, A. K., and Kraus, N. C. (2004). "Two-dimensional depth-averaged circulation model M2D: Version 2.0, report 1, technical document and user's guide." *Technical Rep. No. ERDC/CHL TR-04-2*, U.S. Army Engineer Research and Development Center, Vicksburg, Miss.
- Mory, M., and Hamm, L. (1997). "Wave height, setup, and currents around a detached breakwater submitted to regular or random wave forcing." *Coastal Eng.*, 31, 77–96.
- Nishimura, H. (1988). "Computation of nearshore current." *Nearshore dynamics and coastal processes*, K. Horikawa, ed., University of Tokyo Press, Tokyo, 271–291.
- Péchon, P., et al. (1997). "Intercomparison of wave-driven current models." *Coastal Eng.*, 31, 199–215.
- Reid, R. O., and Bodine, B. R. (1968). "Numerical model for storm surges in Galveston Bay." *J. Wtrwy. and Harb. Div.*, 94(WWI), 33–57.
- Sørensen, O. R., Schäffer, H. A., and Madsen, P. A. (1998). "Surf zone dynamics simulated by a Boussinesq type model. III. Wave-induced horizontal nearshore circulations." *Coastal Eng.*, 33, 155–176.
- Svendsen, I. A. (1984a). "Mass flux and undertow in a surf zone." *Coastal Eng.*, 8, 347–365.
- Svendsen, I. A. (1984b). "Wave heights and set-up in a surf zone." *Coastal Eng.*, 8, 303–329.
- Tajima, Y., and Madsen, O. S. (2006). "Modeling near-shore waves, surface rollers, and undertow velocity profiles." *J. Waterway, Port, Coastal, Ocean Eng.*, 132(6), 429–438.
- Takayama, T., Ikeda, N., and Hiraishi, T. (1991). "Wave transformation calculation considering wave breaking and reflection." *Rept. Port Harbor Res. Inst.*, 30(1), 21–67.
- WAMDI Group. (1988). "The WAM model—a third generation ocean wave prediction model." *J. Phys. Oceanogr.*, 18, 1775–1810.
- Wang, P. (2006). "Measuring longshore sediment transport in a large-scale 3-dimensional laboratory facility." *J. Coastal Res.*, 39, 816–821.
- Wang, P., Ebersole, B. A., and Smith, E. R. (2003). "Beach-profile evolution under spilling and plunging breakers." *J. Waterway, Port, Coastal, Ocean Eng.*, 129(1), 41–46.
- Wang, P., Ebersole, B. A., Smith, E. R., and Johnson, B. D. (2002a). "Temporal and spatial variations of surf-zone currents and suspended sediment concentration." *Coastal Eng.*, 46, 175–211.
- Wang, P., Smith, E. R., and Ebersole, B. A. (2002b). "Large-scale laboratory measurements of longshore sediment transport under spilling and plunging breakers." *J. Coastal Res.*, 18(1), 118–135.
- Watanabe, A., Maruyama, K., Shimizu, T., and Sakakiyama, T. (1986). "Numerical prediction model of three-dimensional beach deformation around a structure." *Coast. Eng. Japan*, 29, 179–194.
- Welch, P. D. (1967). "The use of fast Fourier transformation for the estimation of power spectra: A method based on time averaging over short, modified periodograms." *IEEE Trans. Audio Electroacoust.*, 15, 70–73.
- Zyserman, J. A., and Johnson, H. K. (2002). "Modelling morphological processes in the vicinity of shore-parallel breakwaters." *Coastal Eng.*, 45, 261–284.